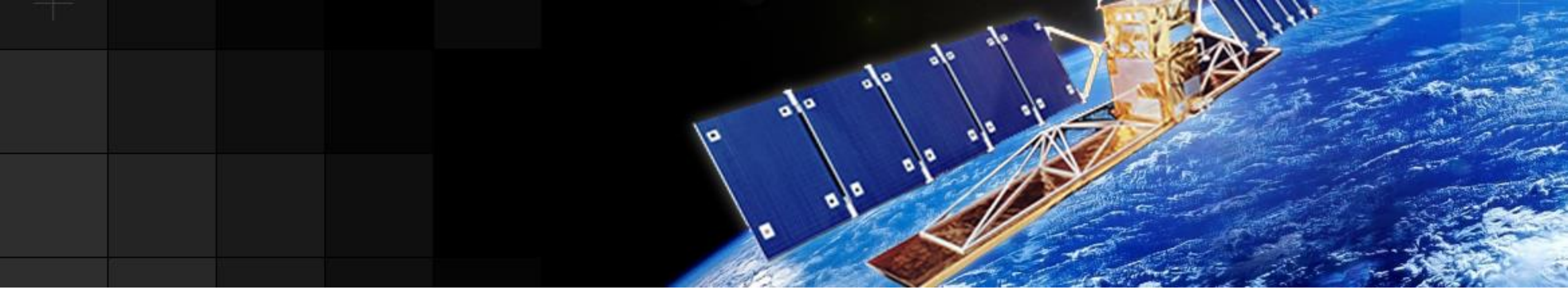

1st International Electronic Conference on Remote Sensing

22 June - 5 July 2015

Investigating Urban Heat Island Estimation and Relation between Various Land Cover Indices in Tehran City Using Landsat 8 Imagery

By: Mahdi Hasanlou and Nikrouz Mostofi

University of Tehran, College of Engineering, Faculty of Surveying and Geospatial Engineering., Tehran, Iran; E-Mail: hasanlou@ut.ac.ir

Islamic Azad University, South Tehran Branch, Department of Surveying Engineering. Tehran, Iran; E-Mail: n_mostofi@azad.ac.ir

Content

- ✓ *Introduction*
- ✓ *Motivation*
- ✓ *Proposed Method*
- ✓ *Experimental Result*
- ✓ *Conclusion*
- ✓ *References*

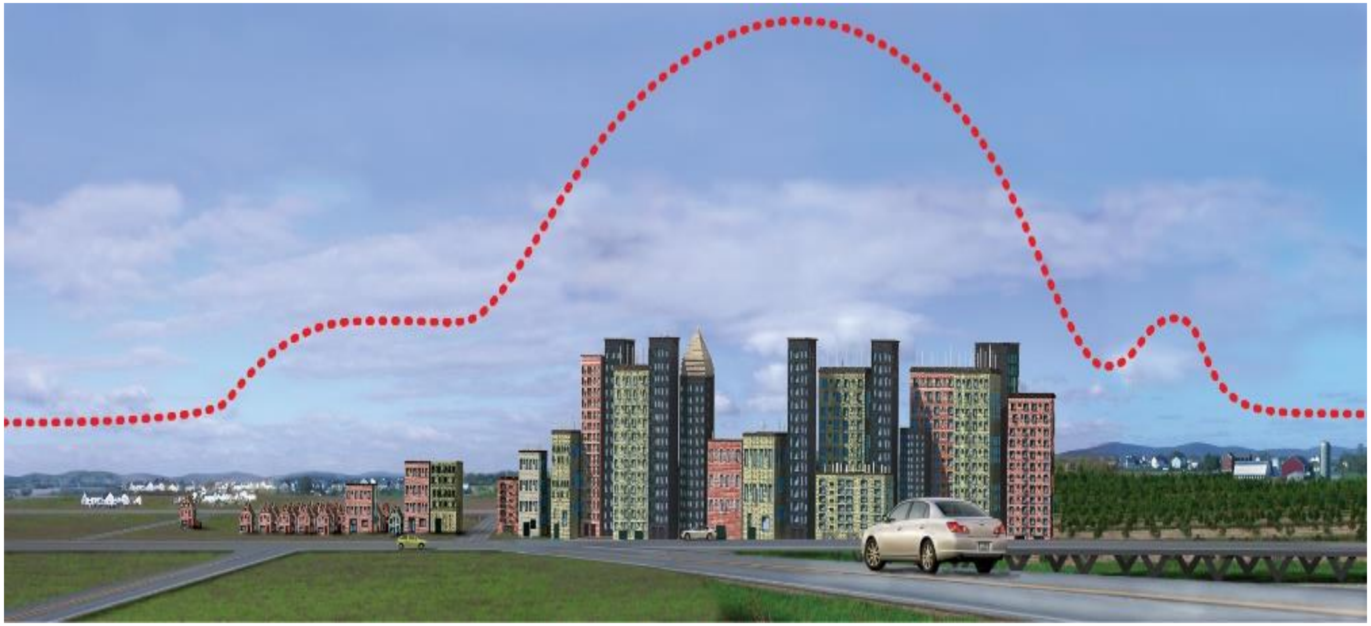

Introduction

Introduction

- ✓ *As urban areas develop, changes occur in the landscape. Buildings, roads, and other infrastructure replace open land and vegetation. Surfaces that were once permeable and moist generally become impermeable and dry.*

- ✓ *This development leads to the formation of urban heat islands (UHI) the phenomenon whereby urban regions experience warmer temperatures than their rural surroundings.*

Introduction

- ✓ *Urban populations are particularly vulnerable due to the UHI phenomenon. City environments hold more heat and routinely experience ambient air temperatures from 2° - 10°F warmer than the surrounding rural and suburban areas. The UHI radiates heat out at night, raising nighttime minimum temperatures, which has been linked epidemiologically with excess mortality.*

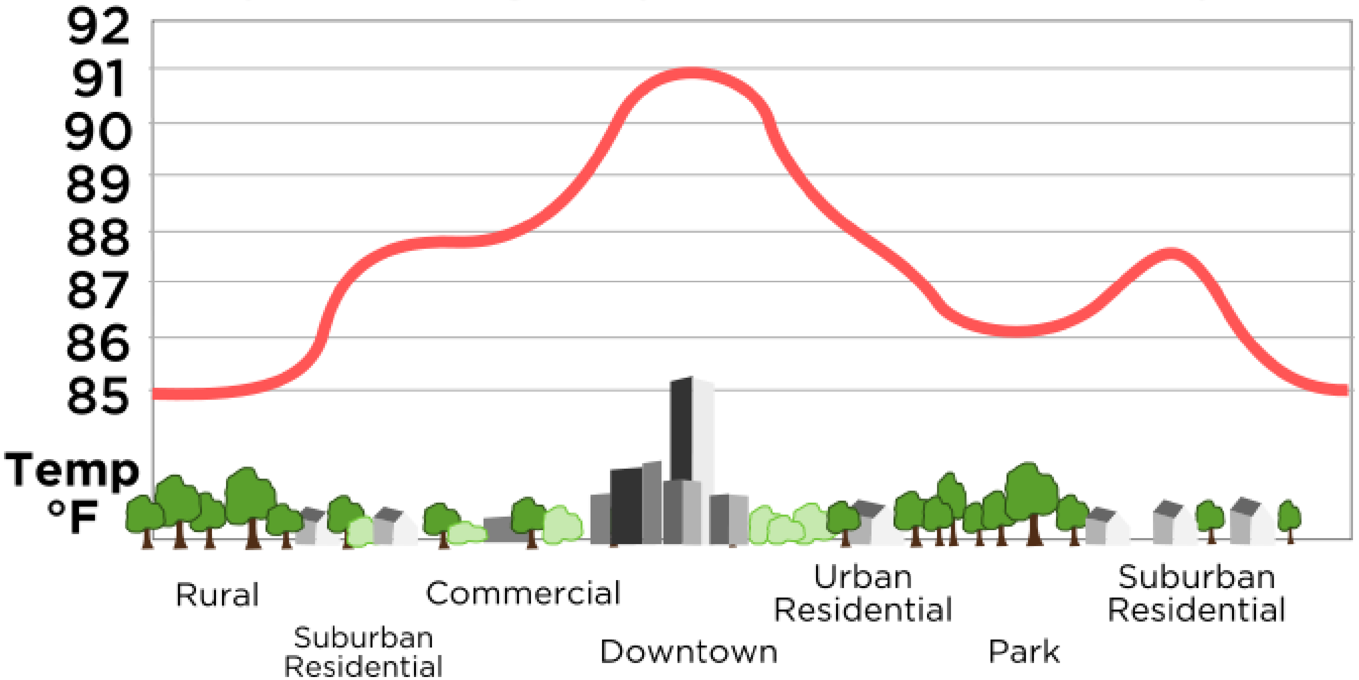

Introduction

Causes of the heat island effect

- ✓ Increased surface water absorption caused by canyon geometry.
- ✓ Decreased LW loss caused by canyon geometry.
- ✓ Increased greenhouse effect caused by air pollution.
- ✓ Anthropogenic heat source.
- ✓ Increased sensible heat storage caused by construction materials.
- ✓ Decreased latent heat flux caused by change of surface type.
- ✓ Decreased sensible and latent heat fluxes caused by canyon geometry (reduction of wind speed).

"Canyons" between buildings

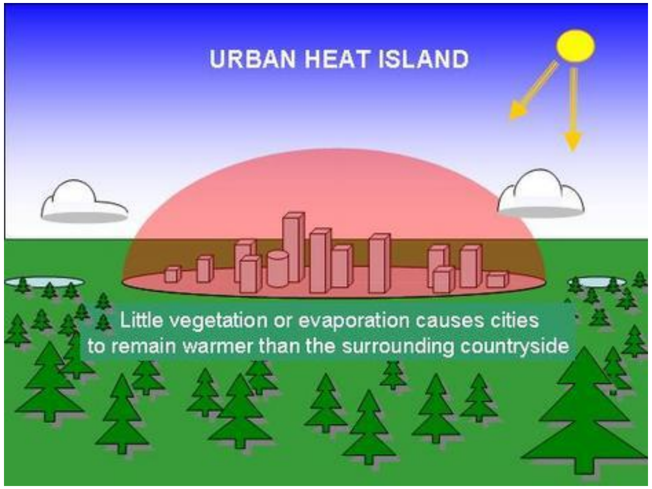

Introduction

Consequences UHI

- ✓ More air conditioning (1-1.5 gigawatts).
- ✓ More electricity, more emission of GHG.
- ✓ More smog.
- ✓ More health problems.
- ✓ Eye irritation, lung damage, asthma.
- ✓ Vegetation issues.

Are there different types of urban heat islands?

✓ *There are three types of heat islands:*

- *Canopy layer heat island (CLHI)*
- *Boundary layer heat island (BLHI)*
- *Surface heat island (SHI)*

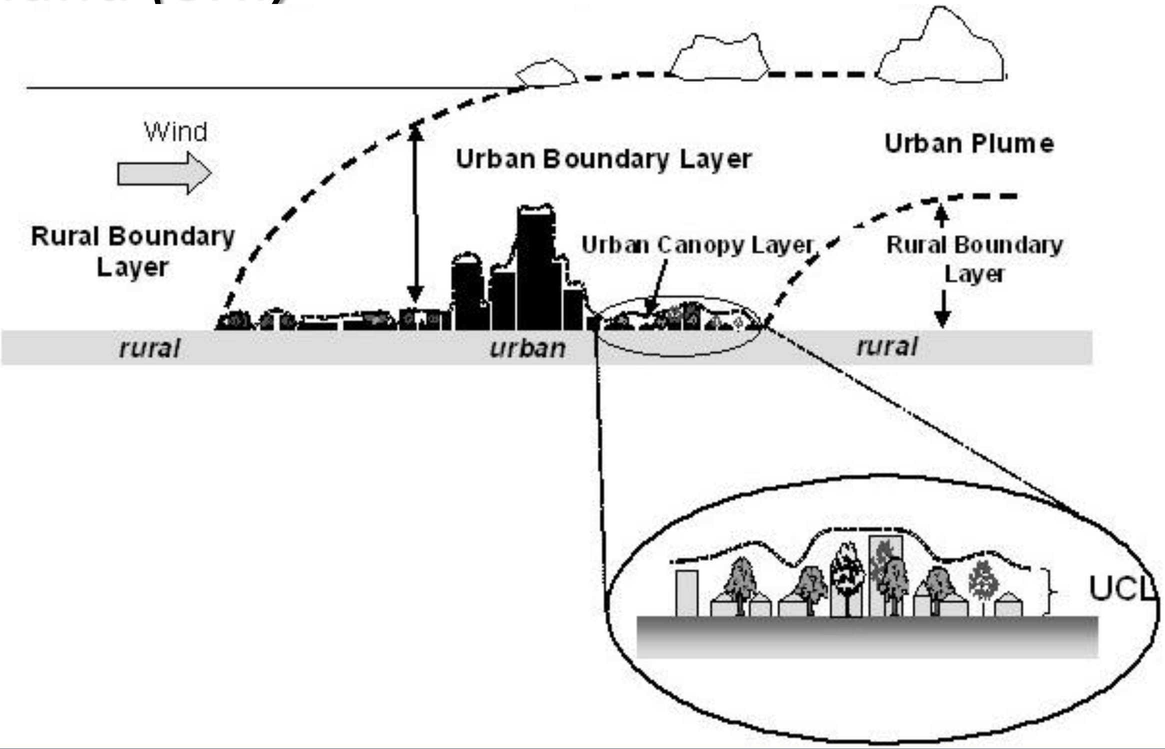

Motivation

Motivation

- ✓ *Investigating mega city (case study Tehran city).*
- ✓ *Investigating Landsat 8 imagery with two valuable Thermal bands (Band 10 and 11).*
- ✓ *Incorporating various urban indices.*
- ✓ *Incorporating various vegetation indices.*
- ✓ *Utilizing kernel base analysis model for urban thermal environment by employing Support Vector Regression (SVR) algorithm.*
- ✓ *Mitigating UHI effects.*

Motivation

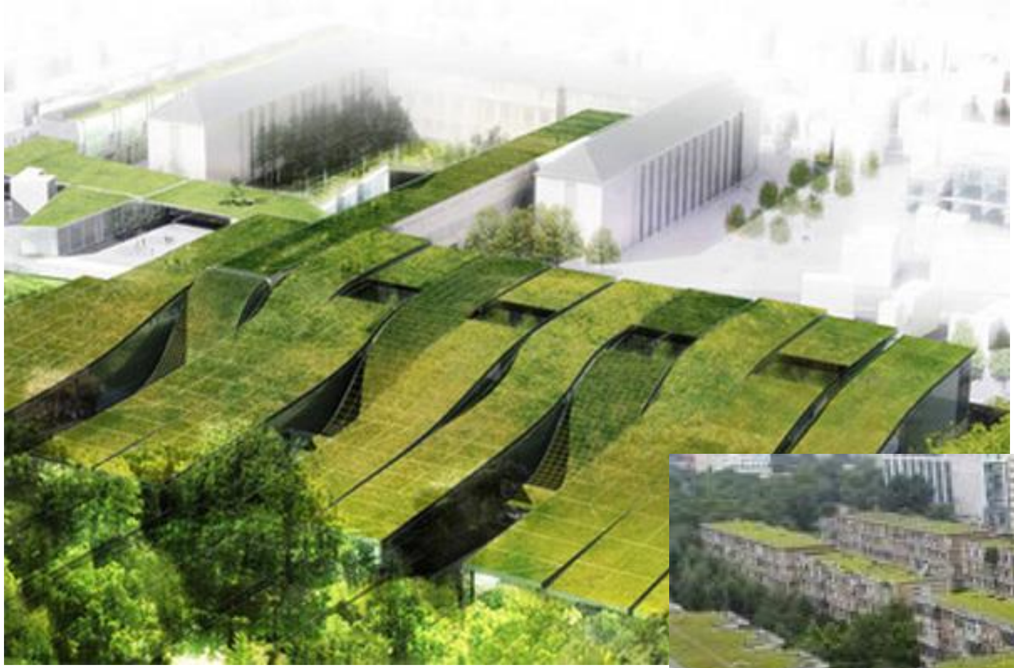

Motivation

✓ Landsat8 - OLI Spectral Bands

Spectral Band	Wavelength	Resolution
Band 1 - Coastal / Aerosol	0.433 - 0.453 µm	30 m
Band 2 - Blue	0.450 - 0.515 µm	30 m
Band 3 - Green	0.525 - 0.600 µm	30 m
Band 4 - Red	0.630 - 0.680 µm	30 m
Band 5 - Near Infrared	0.845 - 0.885 µm	30 m
Band 6 - Short Wavelength Infrared	1.560 - 1.660 µm	30 m
Band 7 - Short Wavelength Infrared	2.100 - 2.300 µm	30 m
Band 8 - Panchromatic	0.500 - 0.680 µm	15 m
Band 9 - Cirrus	1.360 - 1.390 µm	30 m

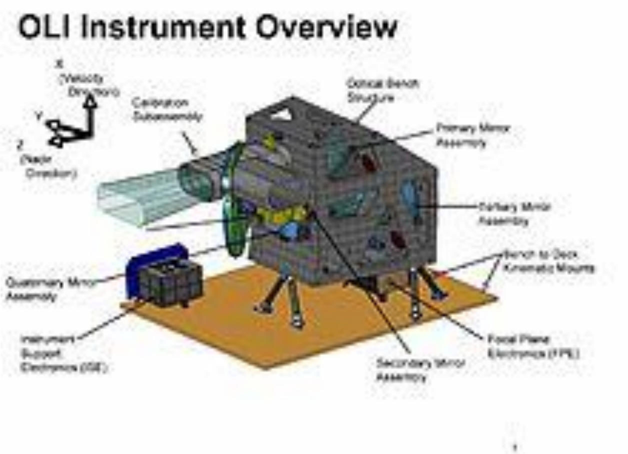

Motivation

✓ Landsat8 - TIRS Spectral Bands

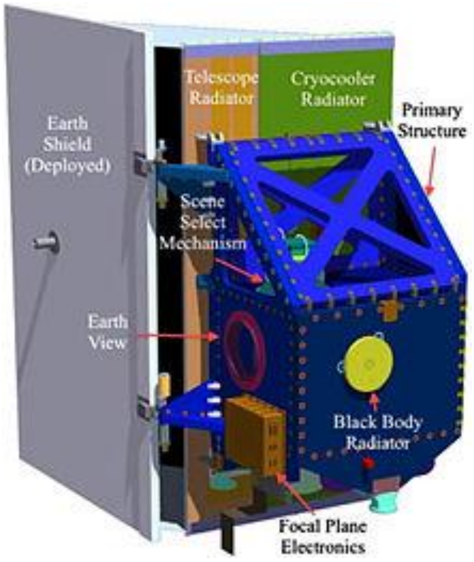

Spectral Band	Wavelength	Resolution
Band 10 - Long Wavelength Infrared	10.30 - 11.30 µm	100 m
Band 11 - Long Wavelength Infrared	11.50 - 12.50 µm	100 m

Motivation

- ✓ *Landsat 8 carries two push-broom instruments: the Operational Land Imager (**OLI**), and the Thermal Infrared Sensor (**TIRS**).*

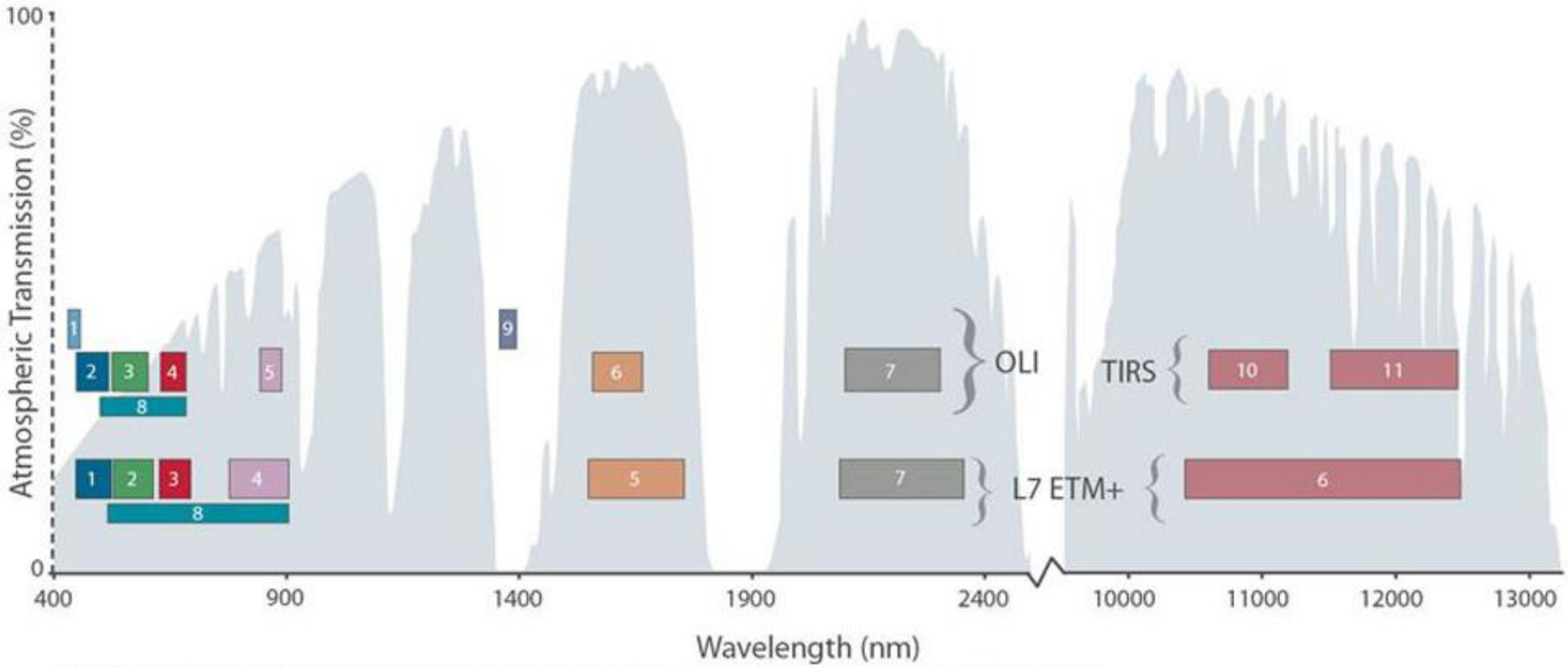

Bandpass wavelengths for Landsat 8 OLI and TIRS sensor, compared to Landsat 7 ETM+ sensor
Note: atmospheric transmission values for this graphic were calculated using MODTRAN for a summertime mid-latitude hazy atmosphere (circa 5 km visibility).

Proposed Method

Proposed Method

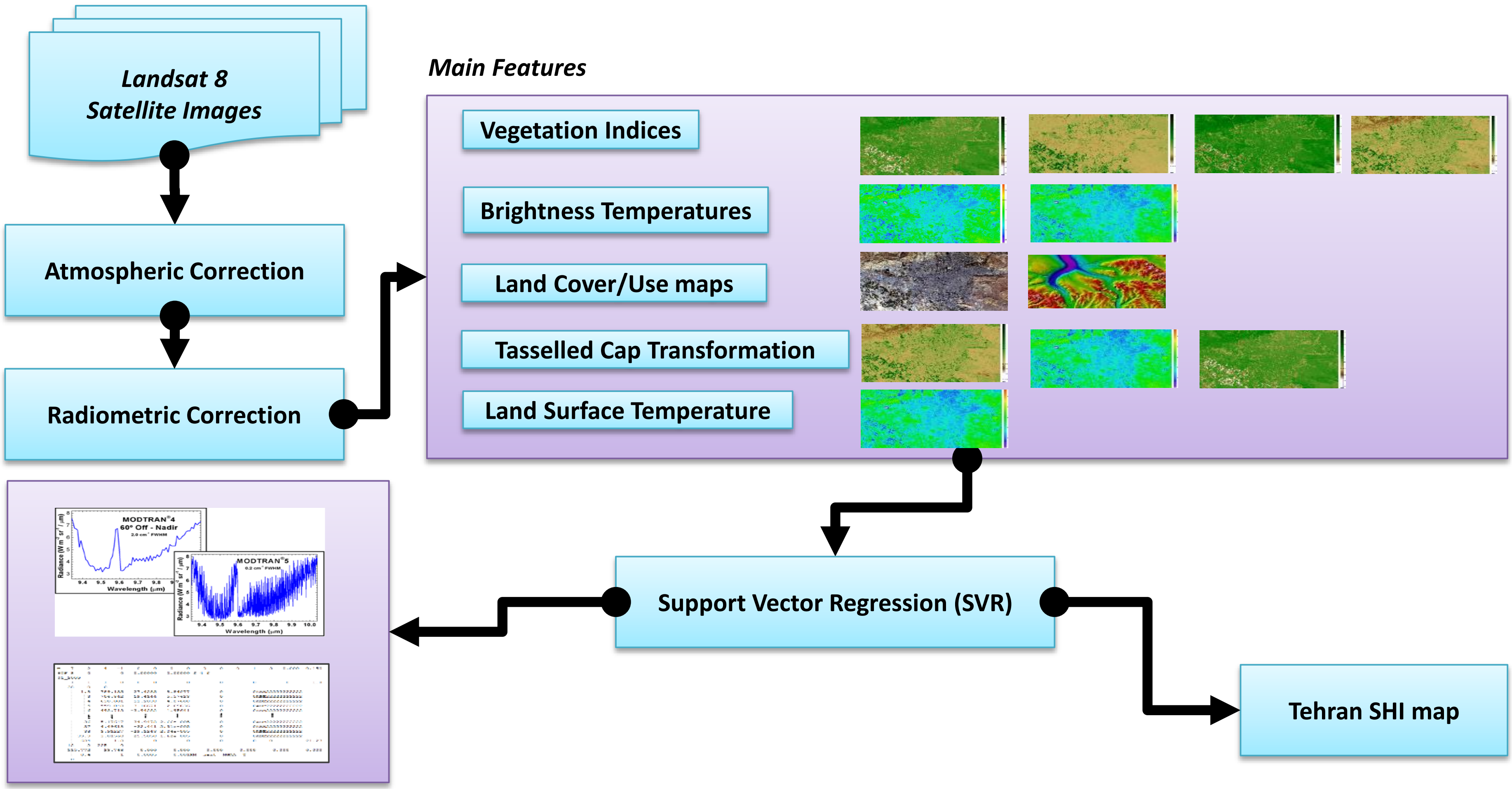

Proposed Method

✓ Urban Indices

No.	Name of urban index	Formulation
1	Normalized Difference Bareness Index (NDBaI)	$NDBaI = \frac{SWIR1 - TIRS1}{SWIR1 + TIRS1}$
2	Normalized Difference Build-up Index (NDBI)	$NDBI = \frac{SWIR1 - NIR}{SWIR1 + NIR}$
3	Bare Soil Index (BI)	$BI = \frac{(SWIR1 + RED) - (NIR + BLUE)}{(SWIR1 + RED) + (NIR + BLUE)}$
4	Urban Index (UI)	$UI = \frac{SWIR2 - NIR}{SWIR2 + NIR}$
5	Index-based Built-Up Index (IBI)	$IBI = \frac{\frac{2\times SWIR1}{SWIR1+NIR} - (\frac{NIR}{NIR+RED} - \frac{GREEN}{GREEN+SWIR1})}{\frac{2\times SWIR1}{SWIR1+NIR} + (\frac{NIR}{NIR+RED} - \frac{GREEN}{GREEN+SWIR1})}$
6	Enhanced Built-Up and Bareness Index (EBBI)	$EBBI = \frac{SWIR1 - NIR}{10\sqrt{SWIR1 + TIRS1}}$

Proposed Method

✓ Vegetation Indices

No.	Name of urban index	Formulation
1	Normalized Difference Vegetation Index (NDVI)	$NDVI = \frac{NIR - RED}{NIR + RED}$
2	Enhanced Vegetation Index (EVI)	$EVI = G \times \frac{NIR - RED}{NIR + C_1 \times RED - C_2 \times BLUE + L}$ $L = 1;\ C_1 = 6;\ C_2 = \ 7.5; G = 2.5$
3	Soil Adjusted Vegetation Index (SAVI)	$SAVI = \frac{NIR - RED}{NIR + RED + L} \times (L + 1)$ $0 < L < 1 \Rightarrow L = 0.5$
4	Normalized Difference Water Index (NDWI)	$NDWI = \frac{NIR - SWIR1}{NIR - SWIR1}$
5	Modified Normalized Difference Water Index (MNDWI)	$MNDWI = \frac{GREEN - NIR}{GREEN + NIR}$
6	Tasselled Cap Transformation (TCT)	Brightness
7	Tasselled Cap Transformation (TCT)	Greenness
8	Tasselled Cap Transformation (TCT)	Wetness

Proposed Method

✓ *Tasselled Cap Transformation (TCT)*

- *Transforms a multi-band image into a series of images optimized for vegetation studies using coefficients specific to a particular sensor*
- *Images represent the “brightness”, “greenness”, and “wetness”*
- *Vegetation studies:*
- *brightness is used to identify and measure soil*
- *greenness is used to identify and measure vegetation*
- *wetness is used to measure soli/vegetation moisture content*

Brightness – Greenness - Wetness

Location for different land cover classes in the B-G spectral space

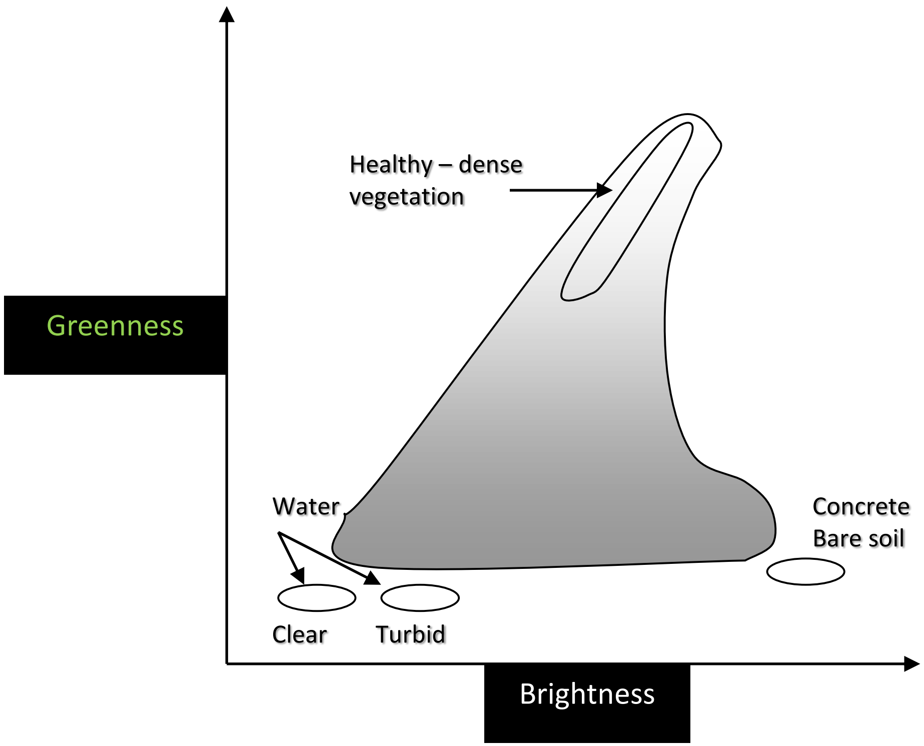

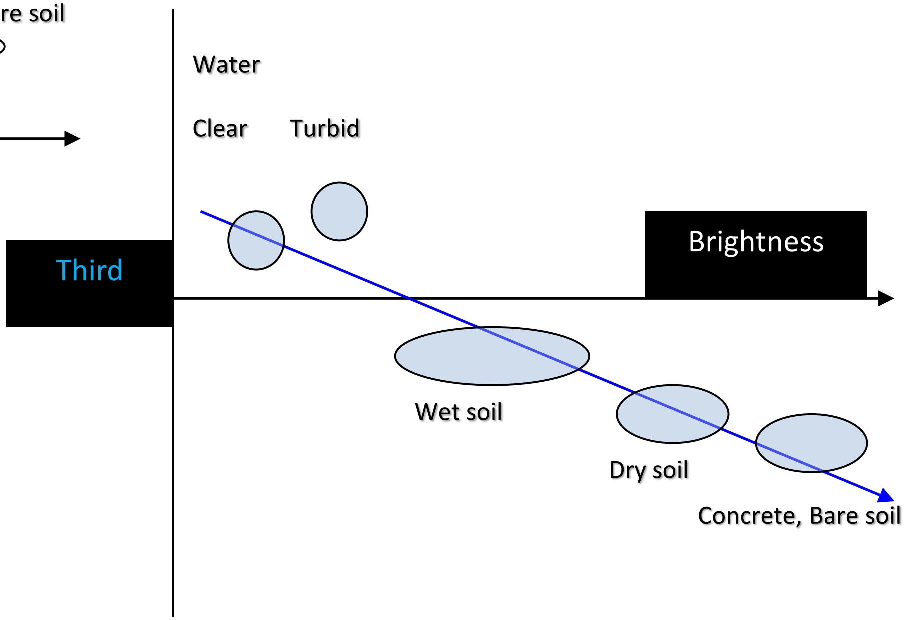

Epsilon Support Vector Regression (ε-SVR)

- *Given: a data set $\{x_1, \ldots, x_n\}$ with target values $\{u_1, \ldots, u_n\}$, we want to do ε-SVR*
- *The optimization problem is*

$$\text{Min } \frac{1}{2}||w||^2 + C\sum_{i=1}^{n}(\xi_i + \xi_i^*)$$

$$\text{subject to } \begin{cases} u_i - \mathbf{w}^T\mathbf{x}_i - b \leq \epsilon + \xi_i \\ \mathbf{w}^T\mathbf{x}_i + b - u_i \leq \epsilon + \xi_i^* \\ \xi_i \geq 0, \xi_i^* \geq 0 \end{cases}$$

- *Similar to SVM, this can be solved as a quadratic programming problem*

Epsilon Support Vector Regression (ε-SVR)

- ✓ *C is a parameter to control the amount of influence of the error*
- ✓ *The $\frac{1}{2}||w||^2$ term serves as controlling the complexity of the regression function*
  - *This is similar to ridge regression*
- ✓ *After training (solving the QP), we get values of α_i and α_i^*, which are both zero if $\mathbf{x}_i$ does not contribute to the error function*
- ✓ *For a new data **z**,*

$$f(\mathbf{z}) = \sum_{j=1}^{s} (\alpha_{t_j} - \alpha_{t_j}^*) K(\mathbf{x}_{t_j}, \mathbf{z}) + b$$

Strengths and Weaknesses of SVR

✓ Strengths of SVR:

- *No local minima*
- *It scales relatively well to high dimensional data*
- *Trade-off between classifier complexity and error can be controlled explicitly via C and epsilon*
- *Overfitting is avoided (for any fixed C and epsilon)*
- *Robustness of the results*
- *The "curse of dimensionality" is avoided*
- *"[Huber (1964) demonstrated that the best cost function over the worst model over any pdf of y given x is the linear cost function. Therefore, if the pdf p(y/x) is unknown the best cost function is the linear penalization over the errors" (Perez-Cruz et al., 2003)*

✓ Weaknesses of SVR:

- *What is the best trade-off parameter C and best epsilon?*
- *What is a good transformation of the original space*

Kernels in SVR

- ✓ *Gaussian radial basis function:*

$$K(\boldsymbol{x}_i, \boldsymbol{x}_j) = \exp(-\gamma \left\| \boldsymbol{x}_i - \boldsymbol{x}_j \right\|^2)$$

- ✓ *Polynomial*

$$K(\boldsymbol{x}_i, \boldsymbol{x}_j) = (\boldsymbol{x}_i \cdot \boldsymbol{x}_j)^d$$

Experimental Result

Experimental Result

✓ *Two Landsat 8 images from Tehran city area*

Dataset	Acquisition date	Area
#1	15-JUN-14	Tehran City
#2	08-DEC-14	Tehran City

Experimental Result

Urban, vegetation and TCT indices for dataset #1

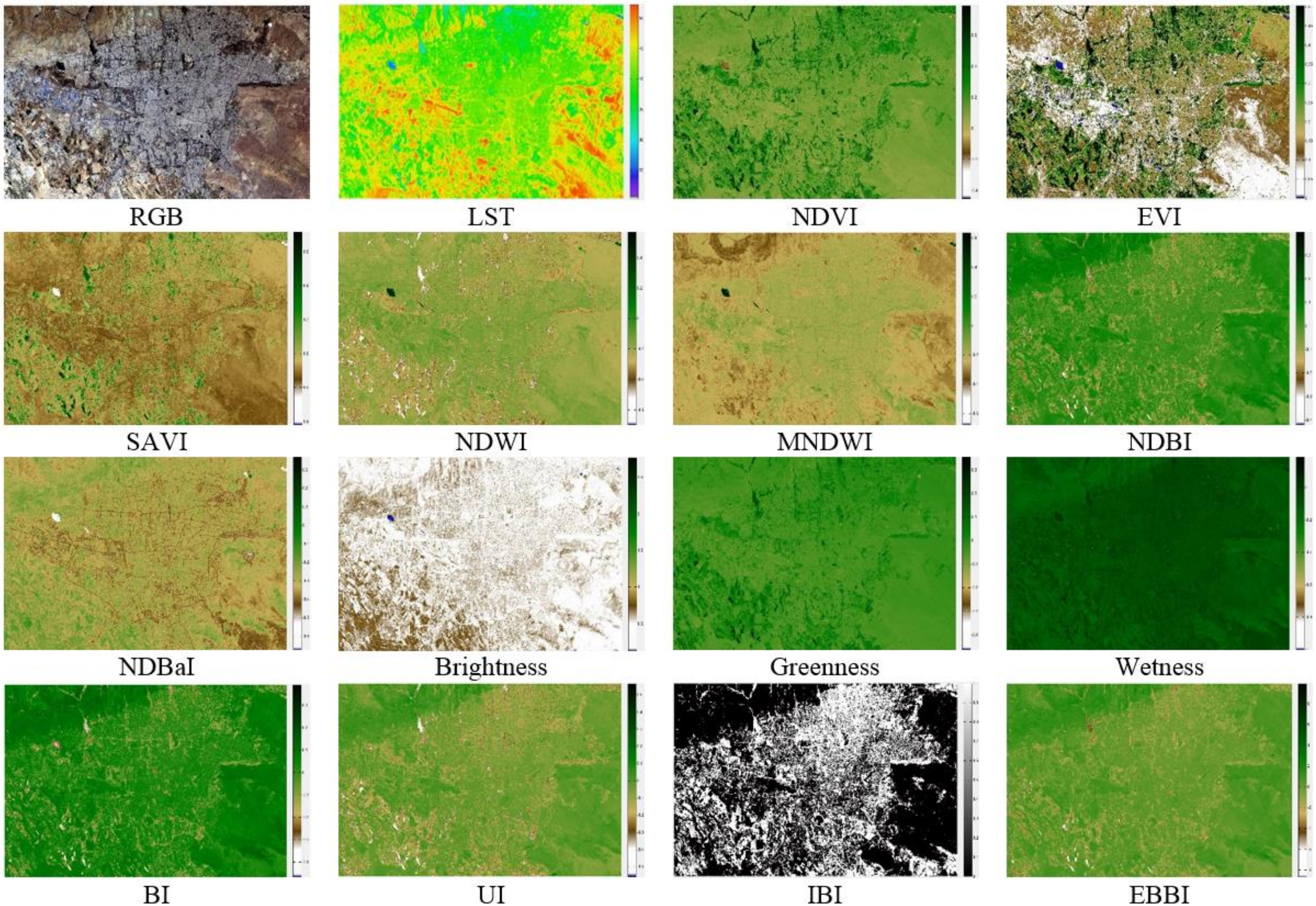

Experimental Result

Urban, vegetation and TCT indices for dataset #2

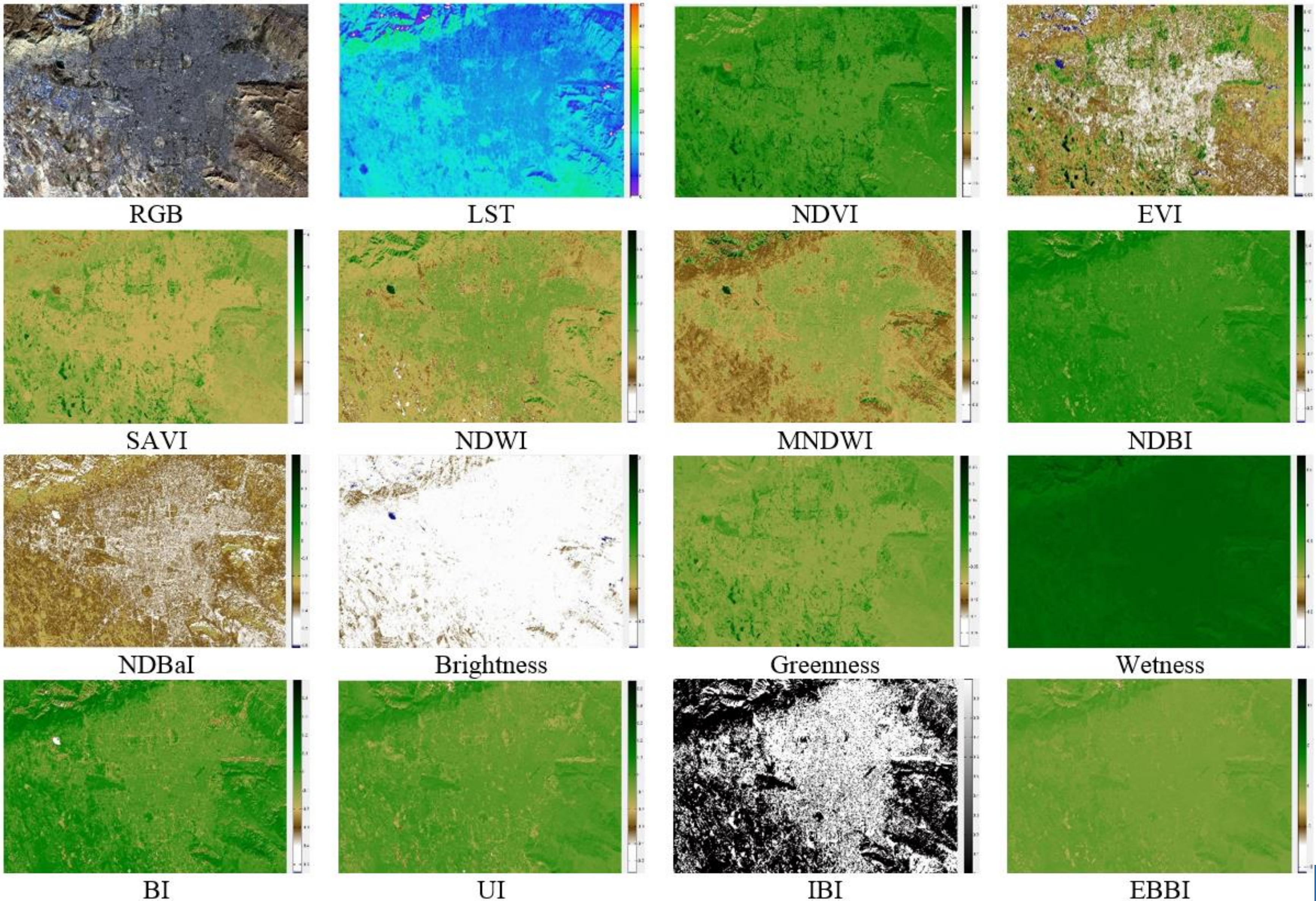

Experimental Result

- ✓ *Model selection in SVR*

$$SHI = f(NDVI, EVI, SAVI, NDWI, MNDWI, Brightness, Greenness, Wetness, NDBaI, NDBI, BI, UI, IBI, EBBI)$$

$$C = \max(Training\ data) - \min(Training\ data)$$

- ✓ *A simple tool to check a grid of parameters is provided by cross-validation (CV) error (i.e. mean square error (MSE)) with 5-fold. Range of grid search method for estimating ε parameter is [0,5] and for γ RBF parameter is $[2^{-7}, 2^{7}]$.*

Experimental Result

Optimum SVR parameters estimation for dataset #1 with C= 22.4013

	$\epsilon = 0$	1	2	3	4	5
$\gamma = 2^{-7}$	8.9248	8.9647	9.044	9.2615	9.4912	9.8826
2^{-6}	8.1931	8.302	8.4365	8.8251	9.0959	9.6601
2^{-5}	7.2267	7.3276	7.672	8.1622	8.5831	9.2708
2^{-4}	5.8522	5.9942	6.6195	7.2668	7.9778	8.76
2^{-3}	3.9949	4.4532	5.2895	6.2399	7.2854	8.105
2^{-2}	2.372	2.9398	3.9742	5.2427	6.397	7.4099
2^{-1}	1.5473	2.1104	3.174	4.4679	5.7297	6.8946
2^{0}	1.4013	1.801	2.8437	4.0502	5.4578	6.598
2^{1}	**1.3833**	1.6836	2.552	3.7709	5.1794	6.5787
2^{2}	1.5092	1.6205	2.4686	3.7119	5.2035	6.759
2^{3}	1.7264	1.8258	2.6858	3.9737	5.3606	7.1223
2^{4}	1.9631	2.2332	3.2883	4.468	5.9297	7.6059
2^{5}	2.4885	2.9571	4.2283	5.5619	6.9744	8.2201
2^{6}	3.554	4.1001	5.4872	6.8119	8.1602	9.2165
2^{7}	5.1897	5.94	7.131	8.2575	9.3713	10.3855

Experimental Result

Optimum SVR parameters estimation for dataset #2 with C= 15.1443

	$\epsilon = 0$	1	2	3	4	5
$\gamma = 2^{-7}$	3.5728	3.6203	3.7465	3.9453	4.2763	4.9328
2^{-6}	3.2757	3.3461	3.5428	3.8146	4.1926	4.8525
2^{-5}	2.8064	2.9516	3.2566	3.6565	4.0248	4.6816
2^{-4}	2.1372	2.3853	2.873	3.4025	3.8541	4.633
2^{-3}	1.3728	1.7408	2.3534	3.1273	3.6953	4.4949
2^{-2}	0.8369	1.214	1.9527	2.8148	3.6012	4.3988
2^{-1}	0.6188	0.9288	1.6741	2.5687	3.51	4.3752
2^{0}	**0.552**	0.7768	1.495	2.4868	3.3917	4.4282
2^{1}	0.5736	0.7643	1.4816	2.4259	3.3971	4.624
2^{2}	0.6387	0.8361	1.5391	2.4159	3.5788	4.9251
2^{3}	0.7551	0.9701	1.7051	2.7299	3.7836	5.0233
2^{4}	0.9101	1.1954	2.0664	3.0564	4.0309	5.0652
2^{5}	1.2115	1.5772	2.4113	3.3655	4.1731	5.2
2^{6}	1.6435	2.0494	2.8103	3.6314	4.4022	5.3901
2^{7}	2.2376	2.6204	3.2666	3.9472	4.6724	5.6117

Experimental Result

The performance of final SVR model for dataset #1

	MSE	NRMS	R^2
Training	0.7507	0.2424	0.9442
Test	1.1155	0.3053	0.9100

The performance of final SVR model for dataset #2

	MSE	NRMS	R^2
Training	0.4307	0.3035	0.9113
Test	0.4546	0.3113	0.9051

Conclusion

Conclusion

- ✓ *All range of Landsat 8 spectral bands have been used for estimating SHI of Tehran city, especially thermal bands.*
- ✓ *In this study, urban indices including NDBaI, NDBI, BI, UI, IBI and EBBI have been calculated using recent urban parameters and factors.*
- ✓ *In addition, for better investigating vegetation factors, more common vegetation and water indices including NDVI, EVI, SAVI, NDWI and MNDWI behind TCT information including Brightness, Greenness and Wetness have been used.*
- ✓ *By utilizing these information and indices modeling and monitoring of SHI are more feasible. Also as part of this study, the powerful regression model, the SVR is used to monitor SHI variation in two different time (dataset #1 and #2) from summer to winter.*
- ✓ *Incorporating this procedure reveled that there is high degree of consistency between affected information and LST images (MSE=0.75 for dataset #1 and MSE=0.43 for dataset #2).*

References

1. Voogt, J. A.; Oke, T. R. Thermal remote sensing of urban climates. Remote Sens. Environ. 2003, 86, 370–384.
2. Xian, G.; Crane, M. An analysis of urban thermal characteristics and associated land cover in Tampa Bay and Las Vegas using Landsat satellite data. Remote Sens. Environ. 2006, 104, 147–156.
3. World's population increasingly urban with more than half living in urban areas | UN DESA | United Nations Department of Economic and Social Affairs.
4. Dihkan, M.; Karsli, F.; Guneroglu, A.; Guneroglu, N. Evaluation of surface urban heat island (SUHI) effect on coastal zone: The case of Istanbul Megacity. Ocean Coast. Manag.
5. Streutker, D. R. A remote sensing study of the urban heat island of Houston, Texas. Int. J. Remote Sens. 2002, 23, 2595–2608.
6. Imhoff, M. L.; Zhang, P.; Wolfe, R. E.; Bounoua, L. Remote sensing of the urban heat island effect across biomes in the continental USA. Remote Sens. Environ. 2010, 114, 504–513.
7. Ogashawara, I.; Bastos, V. da S. B. A Quantitative Approach for Analyzing the Relationship between Urban Heat Islands and Land Cover. Remote Sens. 2012, 4, 3596–3618.
8. Liu, K.; Su, H.; Zhang, L.; Yang, H.; Zhang, R.; Li, X. Analysis of the Urban Heat Island Effect in Shijiazhuang, China Using Satellite and Airborne Data. Remote Sens. 2015, 7, 4804–4833.
9. Fabrizi, R.; Bonafoni, S.; Biondi, R. Satellite and Ground-Based Sensors for the Urban Heat Island Analysis in the City of Rome. Remote Sens. 2010, 2, 1400–1415.
10. Landsat 8 http://landsat.usgs.gov/landsat8.php (accessed May 20, 2015).
11. Actionbioscience | Urban Heat Islands: Hotter Cities http://www.actionbioscience.org/environment/voogt.html (accessed May 20, 2015).
12. Xiong, Y.; Huang, S.; Chen, F.; Ye, H.; Wang, C.; Zhu, C. The Impacts of Rapid Urbanization on the Thermal Environment: A Remote Sensing Study of Guangzhou, South China. Remote Sens. 2012, 4, 2033–2056.
13. Chen, X.-L.; Zhao, H.-M.; Li, P.-X.; Yin, Z.-Y. Remote sensing image-based analysis of the relationship between urban heat island and land use/cover changes. Remote Sens. Environ. 2006, 104, 133–146.
14. Kriegler, F. J.; Malila, W. A.; Nalepka, R. F.; Richardson, W. Preprocessing transformations and their effects on multispectral recognition. In Remote Sensing of Environment, VI; 1969; Vol. 1, p. 97.
15. Huete, A. R. A soil-adjusted vegetation index (SAVI). Remote Sens. Environ. 1988, 25, 295–309.

References

16. Gao, B. NDWI—A normalized difference water index for remote sensing of vegetation liquid water from space. Remote Sens. Environ. 1996, 58, 257–266.

17. Zhao, H.; Chen, X. Use of normalized difference bareness index in quickly mapping bare areas from TM/ETM+. In Geoscience and Remote Sensing Symposium, 2005. IGARSS '05. Proceedings. 2005 IEEE International; 2005; Vol. 3, pp. 1666–1668.

18. Zha, Y.; Gao, J.; Ni, S. Use of normalized difference built-up index in automatically mapping urban areas from TM imagery. Int. J. Remote Sens. 2003, 24, 583–594.

19. Xu, H. Modification of normalised difference water index (NDWI) to enhance open water features in remotely sensed imagery. Int. J. Remote Sens. 2006, 27, 3025–3033.

20. Kawamura, M.; Jayamana, S.; Tsujiko, Y. Relation between social and environmental conditions in Colombo Sri Lanka and the urban index estimated by satellite remote sensing data. Int Arch Photogramm Remote Sens 1996, 31, 321–326.

21. Xu, H. A new index for delineating built-up land features in satellite imagery. Int. J. Remote Sens. 2008, 29, 4269–4276.

22. As-syakur Abd Rahman; Adnyana, I. W. S.; Arthana, I. W.; Nuarsa, I. W. Enhanced Built-Up and Bareness Index (EBBI) for Mapping Built-Up and Bare Land in an Urban Area. Remote Sens. 2012, 4, 2957–2970.

23. Baig, M. H. A.; Zhang, L.; Shuai, T.; Tong, Q. Derivation of a tasselled cap transformation based on Landsat 8 at-satellite reflectance. Remote Sens. Lett. 2014, 5, 423–431.

24. Drucker, H.; Burges, C. J.; Kaufman, L.; Smola, A.; Vapnik, V. Support vector regression machines. Adv. Neural Inf. Process. Syst. 1997, 9, 155–161.

25. Using the USGS Landsat 8 Product http://landsat.usgs.gov/Landsat8_Using_Product.php (accessed May 20, 2015).

26. Jimenez-Munoz, J. C.; Sobrino, J. A.; Skokovic, D.; Mattar, C.; Cristobal, J. Land Surface Temperature Retrieval Methods From Landsat-8 Thermal Infrared Sensor Data. IEEE Geosci. Remote Sens. Lett. 2014, 11, 1840–1843.

27. MOD11A2 | LP DAAC :: NASA Land Data Products and Services https://lpdaac.usgs.gov/products/modis_products_table/mod11a2 (accessed May 22, 2015).

28. Moser, G.; Serpico, S. B. Automatic Parameter Optimization for Support Vector Regression for Land and Sea Surface Temperature Estimation From Remote Sensing Data. IEEE Trans. Geosci. Remote Sens. 2009, 47, 909–921.

29. Durbha, S. S.; King, R. L.; Younan, N. H. Support vector machines regression for retrieval of leaf area index from multiangle imaging spectroradiometer. Remote Sens. Environ. 2007, 107, 348–361.

30. Smola, A. J.; Schölkopf, B. A tutorial on support vector regression. Stat. Comput. 2004, 14, 199–222.

31. Cherkassky, V.; Ma, Y. Practical selection of SVM parameters and noise estimation for SVM regression. 2004, 17, 113–126.

Thanks for your attention

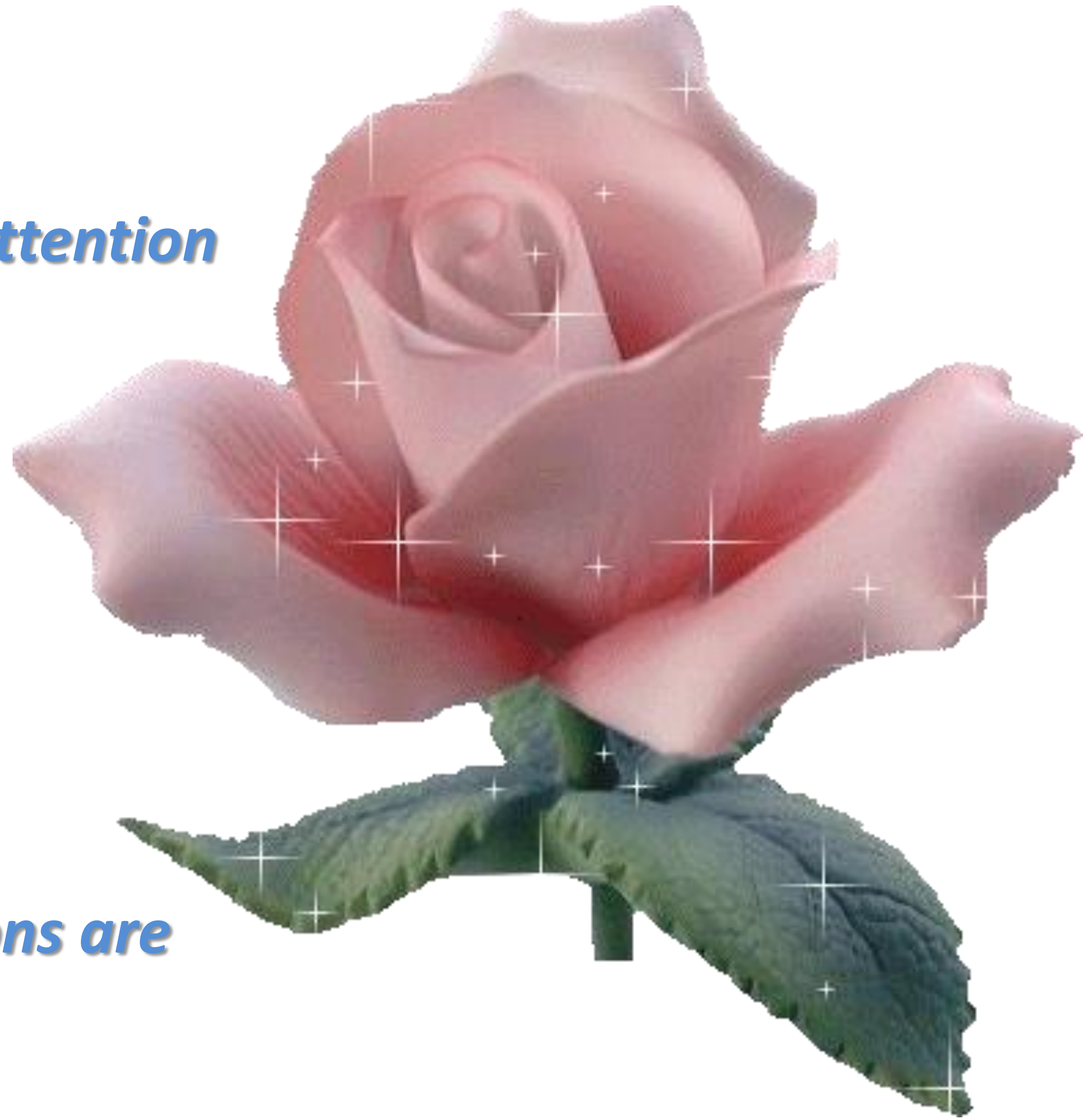

Advices & questions are always welcome!